remote sensing

MDPI

Article

Coastal Dune Invaders: Integrative Mapping of *Carpobrotus* sp. pl. (Aizoaceae) Using UAVs

Michele Innangi [1,†], Flavio Marzialetti [1,†], Mirko Di Febbraro [1,*], Alicia Teresa Rosario Acosta [2], Walter De Simone [3], Ludovico Frate [1], Michele Finizio [1], Priscila Villalobos Perna [1] and Maria Laura Carranza [1]

1 Department of Biosciences and Territory, University of Molise, Contrada Fonte Lappone, 86090 Pesche, Italy
2 Department of Sciences, Roma Tre University, Viale Guglielmo Marconi, 446, 00146 Rome, Italy
3 Department of Life, Health and Environmental Sciences, Environmental Sciences Sect., University of L'Aquila, 67100 L'Aquila, Italy
* Correspondence: mirko.difebbraro@unimol.it; Tel.: +39-0874-4044147
† These authors contributed equally to this work.

Abstract: Coastal dune ecosystems are highly threatened, and one of the strongest pressures is invasive alien plants (IAPs). Mitigating the negative effects of IAPs requires development of optimal identification and mapping protocols. Remote sensing offers innovative tools that have proven to be very valuable for studying IAPs. In particular, unmanned aerial vehicles (UAVs) can be very promising, especially in the study of herbaceous invasive species, yet research in UAV application is still limited. In this study, we used UAV images to implement an image segmentation approach followed by machine learning classification for mapping a dune clonal invader (*Carpobrotus* sp. pl.), calibrating a total of 27 models. Our study showed that: (a) the results offered by simultaneous RGB and multispectral data improve the prediction of *Carpobrotus*; (b) the best results were obtained by mapping the whole plant or its vegetative parts, while mapping flowers was worse; and (c) a training area corresponding to 20% of the total area can be adequate for model building. Overall, our results highlighted the great potential of using UAVs for *Carpobrotus* mapping, despite some limitations imposed by the particular biology and ecology of these taxa.

Keywords: alien early detection; GNDVI; HIS; LSMS; monitoring protocol; OBIA; random forest classification; SAVI; ultra-high spatial resolution

Citation: Innangi, M.; Marzialetti, F.; Di Febbraro, M.; Acosta, A.T.R.; De Simone, W.; Frate, L.; Finizio, M.; Villalobos Perna, P.; Carranza, M.L. Coastal Dune Invaders: Integrative Mapping of *Carpobrotus* sp. pl. (Aizoaceae) Using UAVs. *Remote Sens.* **2023**, *15*, 503. https://doi.org/10.3390/rs15020503

Academic Editors: Francisco Javier Mesas Carrascosa, José Emilio Meroño-Larriva and María Jesús Aguilera-Ureña

Received: 15 December 2022
Revised: 3 January 2023
Accepted: 12 January 2023
Published: 14 January 2023

1. Introduction

Coastal ecosystems, due to their transitional nature between terrestrial and marine environments, are among those with the highest primary and secondary productivity and provide a large number of ecosystem services [1]. At the same time, human activities have had considerable direct and indirect impacts on coastal ecosystems, including habitat reduction, overexploitation, eutrophication, and pollution [2–6]. Beaches and coastal dune systems are among the coastal ecosystems most impacted by human activities, especially tourism-related ones [3,7,8]. Coastal dunes make up about three-quarters of the world's coastline and represent one of the most dynamic landscapes on earth [9,10], providing a multi-service nature of ecosystem services [11]. Under natural conditions, dune systems are characterised by marked gradients in chemical and physical characteristics from the coastline inland, favouring the establishment of highly specialised flora and fauna that follow one another in well-structured and defined communities [8,12–15].

Among the various threats to dune ecosystems, invasive alien plants (IAPs) represent one of the most serious [16]. IAPs are non-native taxa introduced voluntarily or involuntarily by humans, originating breeding populations in places far from their native ranges, resulting in negative economic and/or ecological impacts [17,18]. Indeed, IAPs are considered the second major threat to biodiversity globally, affecting species composition

and jeopardizing the conservation status of invaded habitats [18,19]. Early identification and accurate mapping of the presence of IAPs are basic prerequisites of any containment or eradication plans against these plants [17,20–22], as well as modelling their future invasion risks [23]. Traditional detection and mapping of IAPs usually involve intensive field investigations, which can be time-consuming and costly [24]. Nowadays, the availability of remote sensing technologies enables acquisition of data with more and more spatial and temporal resolution, and have expanded the range of applications in the field of IAPs mapping and detection [25–28]. However, the resolution of most of the satellite data was still recognised as the main cause for classification inaccuracies when discriminating IAPs from native vegetation [29]. An even more innovative frontier is offered by the use of unmanned aerial vehicles (UAVs) that are capable of low flying and acquiring RGB, multispectral, and hyperspectral images at higher resolution than satellite data [30–32]. When it comes to IAPs, resolution of satellite images may not be high enough to detect isolated individual plants or even small populations of plants [33]. In recent years, UAVs have been successfully employed in studying IAPs [32,34–37], sometimes in tandem with satellite imagery or as a high-resolution training dataset for upscaling satellite data [38–41]. Hitherto, despite their potential, the use of UAVs for invasion management of IAPs remains vastly outmatched by satellite and airborne imagery or even field measurements [29].

In coastal dune landscapes, UAVs have proven effective tools in the identification and mapping of IAPs, since the use of satellite imagery alone cannot always yield effective results due to both the dynamic and heterogeneous nature of the landscape and the too coarse spatial resolution compared to the very fine grain of the dunes [34]. Nevertheless, coastal dunes in Europe are more successfully invaded by relatively small species, such as annuals including *Xanthium orientale* L. (Asteraceae) and *Erigeron canadensis* L. (Asteraceae) or several taxa of the genus *Oenothera* L. (Onagraceae) that are biennial hemicryptophytes [42,43]. A recent study showed that 49% of remote sensing applications dealt with the management of herbaceous plant invaders [29], yet most studies addressing herbaceous IAPs are focused on agricultural weeds [44–46]. Moreover, less than 4% of the IAP research has focused on marine coastal sand dune ecosystems, while even less information is available for succulent invaders, which account for about 1.5% of the total IAP studies [29].

Among the succulent IAPs that most seriously threaten dune environments is the genus *Carpobrotus* N.E.Br. (Aizoaceae). Despite their prominent role as invaders on coastal dunes, there is little research on *Carpobrotus* using remote sensing applications [47–50] and, to the best of our knowledge, no studies have ever attempted a detailed, high-resolution mapping of single *Carpobrotus* patches on coastal dunes using a combination of object-based image analysis (OBIA) and machine learning classification based on ultra-high-resolution UAV images.

In this study, we address several technical issues concerning the application of UAVs for identifying and propose potential mapping protocols of *Carpobrotus* invasions on coastal dunes. In particular, we aim to: (a) evaluate the most suitable RS set of variables to predict the presence of *Carpobrotus* among those derived from RGB and multispectral sensors; (b) evaluate the best approach to predict the whole plant or only the green parts or flowers using an OBIA–machine learning approach; and (c) establish the minimum training area in which to carry out photointerpretation of species presence to minimise manual effort when designing monitoring plans in new areas.

2. Materials and Methods

2.1. Study Species

A prominent example of IAP heavily affecting coastal dunes is the genus *Carpobrotus* (Figure 1). *Carpobrotus* are succulent, trailing perennial grasses, native to South Africa with a great propensity for clonal reproduction [51–53]. They have been introduced to Europe for ornamental and soil stabilisation purposes since the early 17th century and they are now widely naturalised in coastal habitats of southern and western Europe [53]. Two different species are typically found in Europe: *C. edulis* (L.) N.E.Br. and *C. acinaciformis* (L.) L.Bolus,

which are often difficult to distinguish from each other and can easily hybridise [49,53]. Although it is problematic to discriminate between the two species (especially in the absence of flowers), their ecological impact is essentially the same [54]; thus, from now onwards, we refer to *Carpobrotus* indicatively.

Figure 1. UAV image of a single patch of *Carpobrotus* about 6 m in diameter, with details of the plant as a whole, the green parts, and the flowers. Pictures by Michele Innangi.

Carpobrotus can invade sandy coastal ecosystems—from embryonic dunes to juniper groves—and rocky coastal ecosystems with equal success [53]. *Carpobrotus* represents one of the most important plant invaders in the Mediterranean [53,55], where their spread in coastal ecosystems is seriously threatening the conservation of biodiversity on both local and global scales, and numerous eradication initiatives have been implemented [56], especially on small islands [55,57,58].

2.2. Study Area

The area under investigation was a sector of central Italy on the Thyrrenian coast (41.909461°N, 12.148823°E, Passoscuro, Fiumicino, Rome; Figure 2). In this area, it is possible to recognise the typical dune zonation characterised by a strong environmental gradient from the coastline inland that contributes to the formation of a sequence of habitats, many of which are of conservation importance [3,13,14]. In spite of the presence of a well-formed dune structure, the Passoscuro area has also been subject to tourist exploitation, encouraging a strong colonisation of alien species, in particular *Carpobrotus* [41].

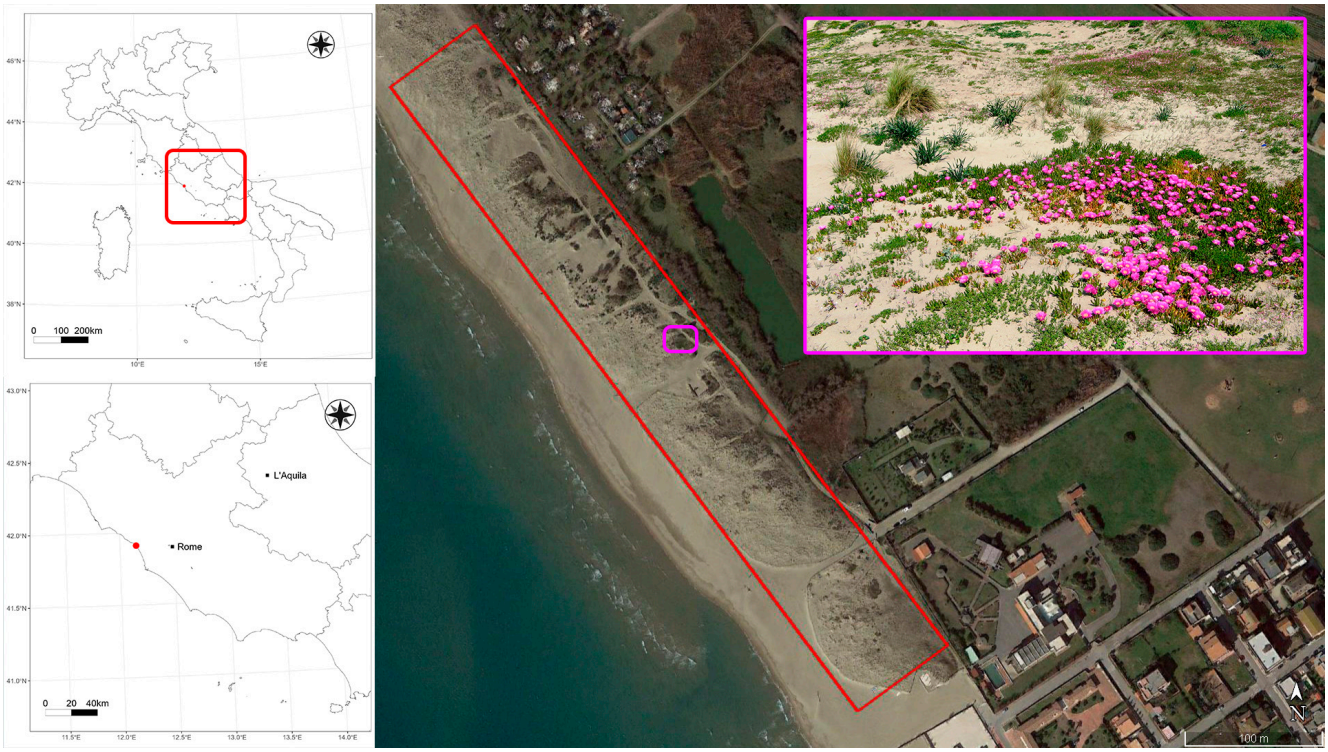

Figure 2. Map of the study area (41.909461°N, 12.148823°E, Passoscuro, Fiumicino, Rome, EPSG:4326-WGS84). The location of the Passoscuro shoreline where the UAV surveys were carried out is shown in the red boxes on the left on a map of Italy and a map of the region Latium where Passoscuro is located. The 5-hectare area surveyed is outlined in red in the central air photo (image acquired in March 2022 © Maxar Technologies and visible on the © Google Earth platform). The top right inset shows detail of the Passoscuro dune, highlighting a *Carpobrotus* bloom (Picture by Alicia Teresa Rosario Acosta).

2.3. Data Acquisition and Pre-Processing

We implemented a semi-automatic classification approach based on OBIA followed by machine learning classification for mapping *Carpobrotus*. An outline of the whole methodology can be seen in Figure 3. In May 2021 (i.e., during the peak flowering period of *Carpobrotus*), images were acquired by a UAV equipped with two different sensors over an area of approximately 5 hectares. We employed a multirotor quadcopter DJI Phantom 4 Pro V2.0 equipped with CMOS (complementary metal oxide semiconductor) sensor, i.e., a Red–Green–Blue (RGB) camera with 20 Mpx and 24 mm of equivalent focal length (EFL), and Parrot Sequoia multispectral camera with four bands, each with 1.2 Mpx and 30 mm EFL: Green (G, bandwidth: 550 nm $\pm$ 40 nm), Red (R, bandwidth: 660 nm $\pm$ 40 nm), Red Edge (RE, bandwidth: 735 nm $\pm$ 10 nm), and Near Infrared (NIR, bandwidth: 790 nm $\pm$ 40 nm).

Flights were planned via the freeware mobile application PIX4Dcapture (version 4.11.0 for Android, https://www.pix4d.com/product/pix4dcapture/, accessed on 18 November 2022). All UAV surveys were standardized using the same settings: time of acquisition between 10:00 and 12:00 PM, altitude of 35 m above the take-off point and speed of 5 m/s. The image overlap was set to 80% for both forward and lateral overlap. For setting up the Parrot Sequoia camera, we used the dedicated HTML interface, accessible by connecting the camera to the smartphone via Wi-Fi. Within the HTML interface, we entered the same flight altitude and image overlay values described for the PIX4Dcapture application. The two sensors captured images simultaneously during the flights; the CMOS sensor was activated by PIX4Dcapture, while the Parrot Sequoia camera was activated by the HTML interface. Before the flights, 12 ground control points (GCPs) of 50 cm^2 were placed in the flight area. The coordinates of the GCPs (longitude, latitude, and

altitude) were measured with a high-precision GNSS receiver (Trimble R2) connected to the HxGN SmartNet GNSS positioning services for RTK correction (nearest) with nominal and estimated horizontal accuracies of 1 and 7 cm, respectively. All aerial images were processed using Agisoft Metashape Professional's Structure for Motion (SfM) approach (version 1.6.2, https://www.agisoft.com/, accessed on 18 November 2022). We produced, for each flight, the RGB orthomosaic and the digital surface model (DSM) using the aerial images derived from the RGB CMOS sensor and the orthomosaics of the G, R, RE and NIR bands from the aerial images of the multispectral Parrot Sequoia sensor. These orthomosaics were georeferenced with the coordinates of the GCPs [34,59,60]. The spatial resolutions were 2 cm in RGB orthomosaics, 2.5 cm in DSM, and 5 cm in multispectral orthomosaics. All orthomosaics were upscaled by means of bilinear interpolation to a resolution of 5 cm, which was the coarsest resolution available from the multispectral data [34,61].

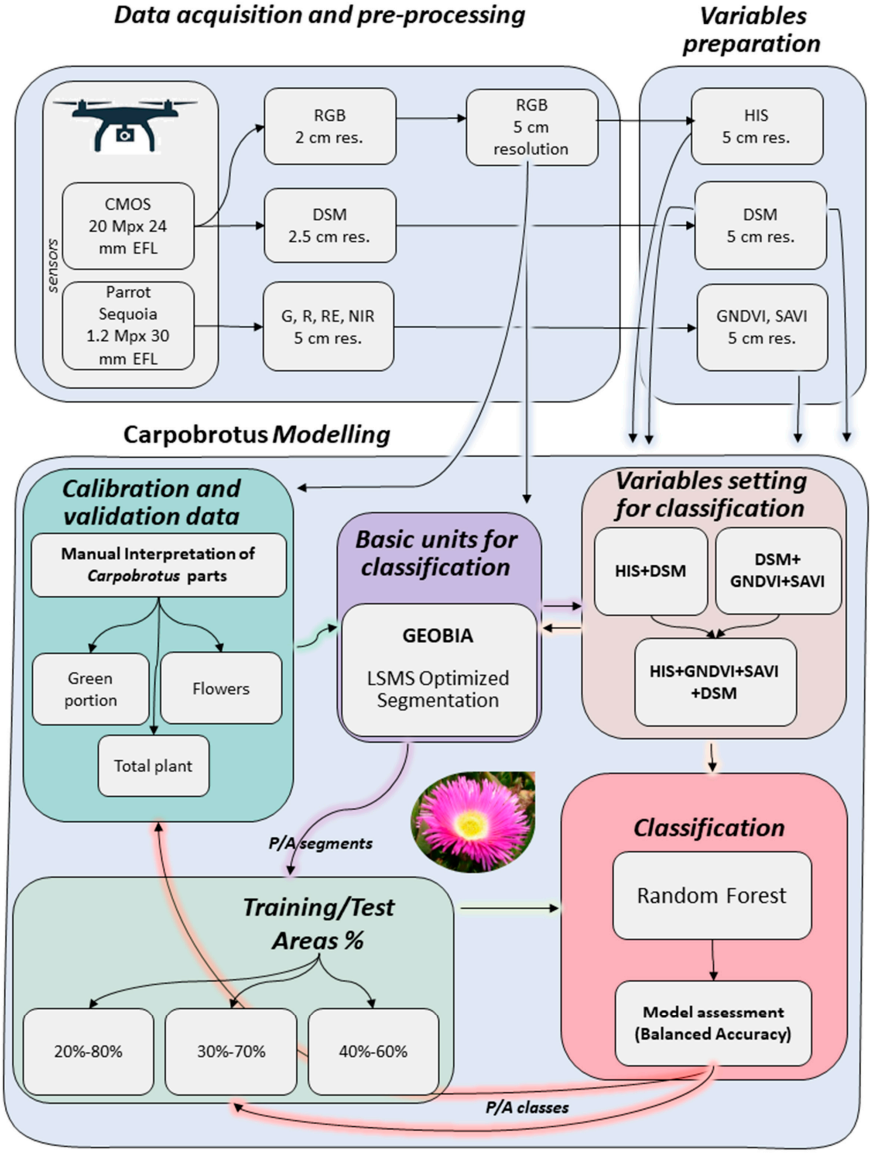

Figure 3. Simplified outline of the semi-automatic classification approach based on OBIA followed by machine learning classification adopted in this study. For details, see Section 2.

2.4. Preparation of Variables

Based on the up-scaled RGB orthomosaic, we derived hue, intensity, and saturation metrics (HIS) using the *i.rgb.his* tool within GRASS GIS 8.2 (https://grass.osgeo.org/, accessed on 19 November 2022), where hue (HUE) refers to the dominant wavelength of

light within the pixel, intensity (INT) refers to the total brightness of a colour measured as the relative degree of black or white, while saturation (SAT) refers to the purity of colour defined as the absence of blending in a fully saturated pixel devoid of other frequencies [34,62]. Based on the multispectral orthomosaics, we derived two indexes that have been listed among those useful for detecting alien species [27], i.e., green normalized difference vegetation index (GNDVI, Equation (1)) and soil adjusted vegetation index (SAVI, Equation (2)). GNDVI is derived from the normalized difference vegetation index (NDVI) but, while NDVI involves NIR and R bands, GNDVI involves NIR and G bands [63]. GNDVI was shown to have a larger dynamic range than the NDVI, strong sensitivity to chlorophyll concentration across vegetation [63], and was successfully employed to study biodiversity and alien species [32,64]. SAVI was also introduced as a modification of NDVI, yet this index aimed to reduce soil brightness influences from spectral vegetation indices involving R and NIR wavelengths [65]. This correction is made by introducing the L factor into the index, which is set at 0.5 when there is little or intermediate vegetation [65]. SAVI was shown to be the most important spectral indices in predicting alien species distribution in arid ecosystems [66], aridity that also characterises dune systems.

$$\mathrm{GNDVI} = \frac{\mathrm{NIR} - \mathrm{G}}{\mathrm{NIR} + \mathrm{G}} \quad (1)$$

$$\mathrm{SAVI} = \frac{\mathrm{NIR} - \mathrm{R}}{\mathrm{NIR} + \mathrm{R} + \mathrm{L}} \times (1 + \mathrm{L}) \; with \; \mathrm{L} = 0.5 \quad (2)$$

HIS, multispectral indexes (GNDVI and SAVI, which we refer to simply as multi) and DSM data were all rescaled between the values of 0 and 255 [34,67] to reduce potential errors in the classification algorithm due to the different units of measurement of the variables.

Calibration and validation data were produced though photointerpretation of the original RGB image at a resolution of 5 cm. After masking artificial infrastructures (e.g., buildings or previously built-up areas, construction sites, roads, etc.) all recognisable *Carpobrotus* plants were manually interpreted on video with the help of QGIS 3.28 (https://www.qgis.org/, accessed on 17 November 2022), distinguishing between the flowers and green parts of the plant. In this way, we obtained a dataset able to depict the whole plant (i.e., Total plant), the green parts only (i.e., Green), and the flowers (i.e., Flowers).

2.5. Carpobrotus Modelling

We ran a total of 27 classification models, combining three different sets of RS variables (i.e., HIS + DSM, Multi + DSM, HIS + Multi + DSM), the different parts of the plant (i.e., Total plant, Green portions, and Flowers), and incremental calibration areas (i.e., 20–30–40% of the whole area). Specifically, calibration was implemented using incremental belts of the study area starting from the centre (i.e., 20–30–40% of the whole area), while the remaining portions were used for model validation (i.e., 80–70–60% of the whole area).

For every model, we generated the basic units for the classification by image segmentation of the original RGB orthomosaic using a geographic object-based image analysis approach (GEOBIA) [34,68]. Specifically, we used the large scale mean shift (LSMS) algorithm implemented in the open–source software Orfeo Toolbox for image classification [69]. The LSMS is a non-parametric, iterative clustering algorithm that groups image regions based on spatial and spectral proximity into homogeneous segments. The algorithm needs three parameters for optimal performance: spatial radius (sr), defining the maximum Euclidean spatial distance between pixels to be grouped in the same polygon; range radius (rr), the maximum Euclidean spectral distance between pixels to be grouped in the same polygon; and minimum segment size (ms), the minimum number of pixels per segment to define a polygon. We optimised the selection of segmentation parameters using an iterative algorithm. Initially, we created all possible combinations of the three LSMS parameters considering the following ranges: sr 1–14, rr 1–14, and ms 30–140 for total and green parts of *Carpobrotus* and rs 1–10, rr 1–10, and ms 10–50 for flowers. These values have been

chosen based on previous literature [30,34,68,70] to account for the different sizes of the plant's parts. From this set of combinations, we selected a random 20% and used it as an initial screening by performing the segmentation of the original RGB orthomosaic over the largest training area (40%). Then, we selected only the five combinations of LSMS parameters that gained the highest internal validation metric (mean balanced accuracy 0.835 $\pm$ 0.077) and we repeated the previous step. At the end of the process, we identified the best LSMS parameters per each model. Subsequently, the optimised segments were classified *Carpobrotus* presence when at least 50% of the pixels in them had been photo-interpreted as *Carpobrotus*, while the remaining segments were classified as absences.

Subsequently, for each model, 20% of the whole segment was used for calibration using random forest (RF), a machine learning regression/classification algorithm that works by constructing a large number of decision trees to generate spatial classifications and predictions [15,34,71]. We used the method 'ranger' as RF algorithm, implemented in the 'caret' R package [72]. RF classification models were optimally-tuned through internal 10-fold cross validation [73]. Specifically, the number of uncorrelated decision tress (Ntree) was set to 1000, while we tested for the highest accuracy in terms of optimal split rules and for the number of variables randomly selected at each node of decision trees (Mtry, ranging from two to the max number of variables within each model). The Gini index for classification (impurity) was used to assess variable importance. Finally, the calibrated model was projected on the test areas.

The accuracy of the models was quantified by assessing model predictions against the *Carpobrotus* presence-absence segments on the test areas (i.e., that were held out from the model calibration). In particular, given the strong class imbalance occurring between *Carpobrotus* presence and absence segments, we chose to rely on the balanced accuracy (BA) as an overall predictive performance metric. BA is an unbiased metric ranging from 0 to 1 and it is computed as the arithmetic mean between the true positive rate (sensitivity) and the true negative rate (specificity). BA values below 0.5 can be considered as indicating a random prediction. BA was shown to be a reliable metric when there is a strong class imbalance in several binary classification scenarios, including with remote sensing data [74–76]. From a computational point of view, BA is equivalent to true skill statistics (TSS), which is the sum of sensitivity and specificity minus one, and as a consequence, TSS can also assume negative values [77,78]. BA values can be computed from TSS by a simple linear equation ($BA = \frac{1}{2} \times TSS + \frac{1}{2}$).

Lastly, we assessed which factor (i.e., the combination of RS variables, the part of the plant analysed, and the percentage of the training area) was more decisive in influencing BA values by fitting a linear model that included BA as the response variable and the different factors and their combinations as covariates. The residuals of this model were checked for linearity and homoscedasticity. All statistical analyses were performed using R version 4.2.1. [79] using packages 'caret' [72], 'SegOptim' [80], and 'terra' [81].

3. Results

The results for the LSMS optimization can be seen in Figure 4. The parameters were very similar with regard to the analysis of the plant in its entirety (Total), with few differences depending on the type of variables used. In particular, sr was optimal between 1 and 2, rr between 10 and 12, and ms between 110 and 150. The analysis on the green parts of the plant alone (Green), on the other hand, resulted in a change about rr, which was lower (between 2 and 4) when multispectral data were present in the dataset, while sr and ms were comparable at Total. Finally, the case of flowers showed the greatest variability with different results depending on the type of dataset used and characterised above all by higher sr values, up to 10 in the case of Multi + DSM.

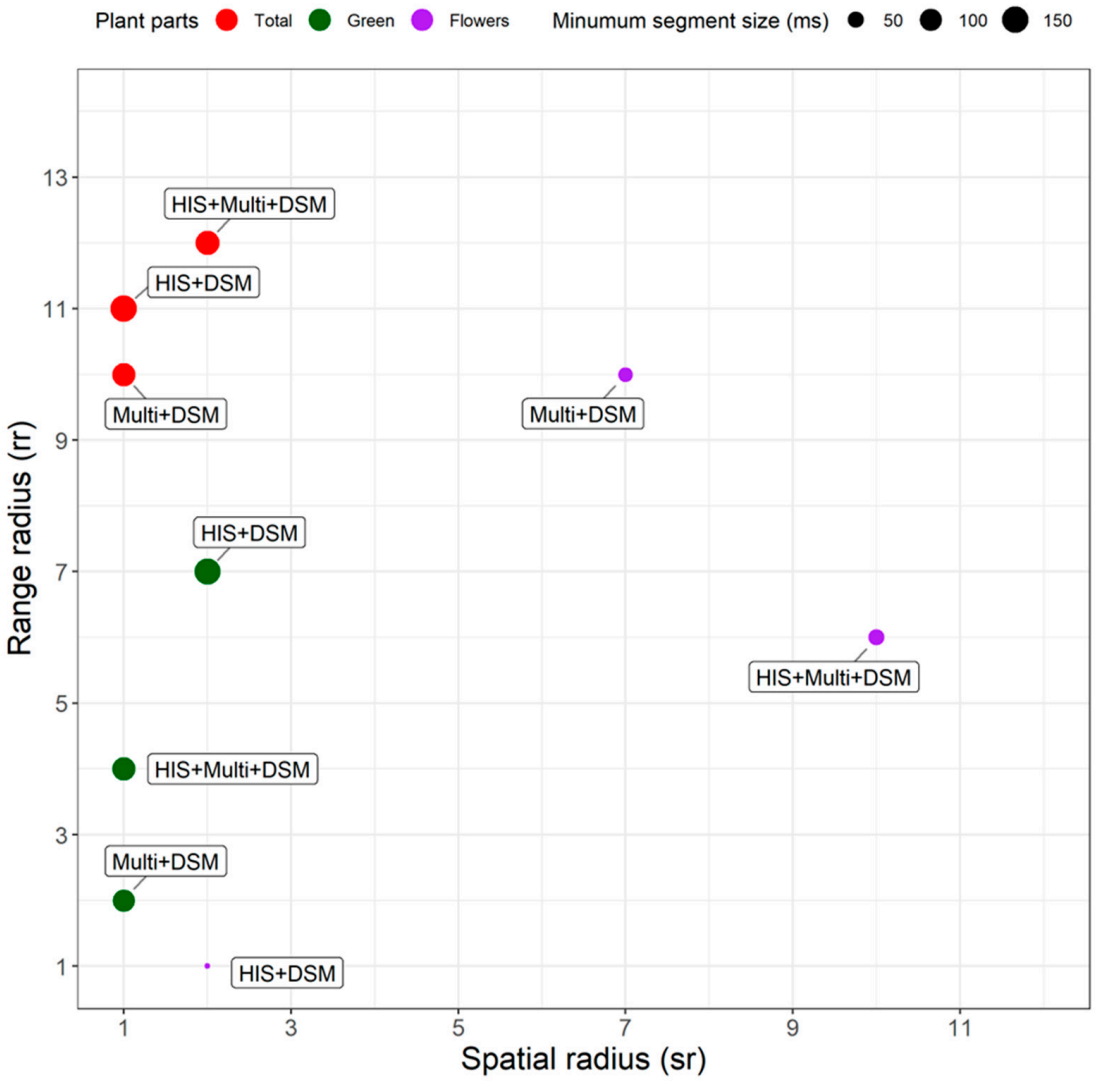

Figure 4. Graphical representation of optimised LSMS segmentation parameters. The x and y axes represent spatial radius (sr) and range radius (rr), respectively, while the point size is given by minimum segment size (ms). The points are also coloured according to the different parts of the plant analysed and bear the labels for the variable dataset used for optimisation.

The highest balanced accuracy values were gained for both Total (BA 0.689 ± 0.006) and Green parts (BA 0.686 ± 0.007) using the combination of HIS + Multi + DSM, which was marginally better than HIS + DSM (BA 0.677 ± 0.008 and 0.680 ± 0.005 for Total and Green parts, respectively), although differences were not significant (Figure 5; Table 1). Multi + DSM showed the lowest BA values (BA 0.565 ± 0.012 and 0.575 ± 0.014 for Total and Green parts, respectively), although the model highlighted that this set of variables significantly increased the BA for Flowers (BA 0.530 ± 0.010 compared to 0.513 ± 0.006 with HIS + DSM and similar to 0.530 ± 0.022 for HIS + Multi + DSM; Figure 5; Table 1).

The factor that most affected BA was the part of the plant analysed, with comparable values between the Total and the Green parts, while average values were significantly lower by a factor of 0.16 for the Flowers. Regarding the type of data used to calibrate the models, the results show no significant difference between HIS + DSM and HIS + Multi + DSM, while the results obtained by Multi + DSM were significantly lower, reducing BA by 0.11. Finally, despite some differences visible in Figure 5, the differences due to the size of the calibration area were not statistically significant.

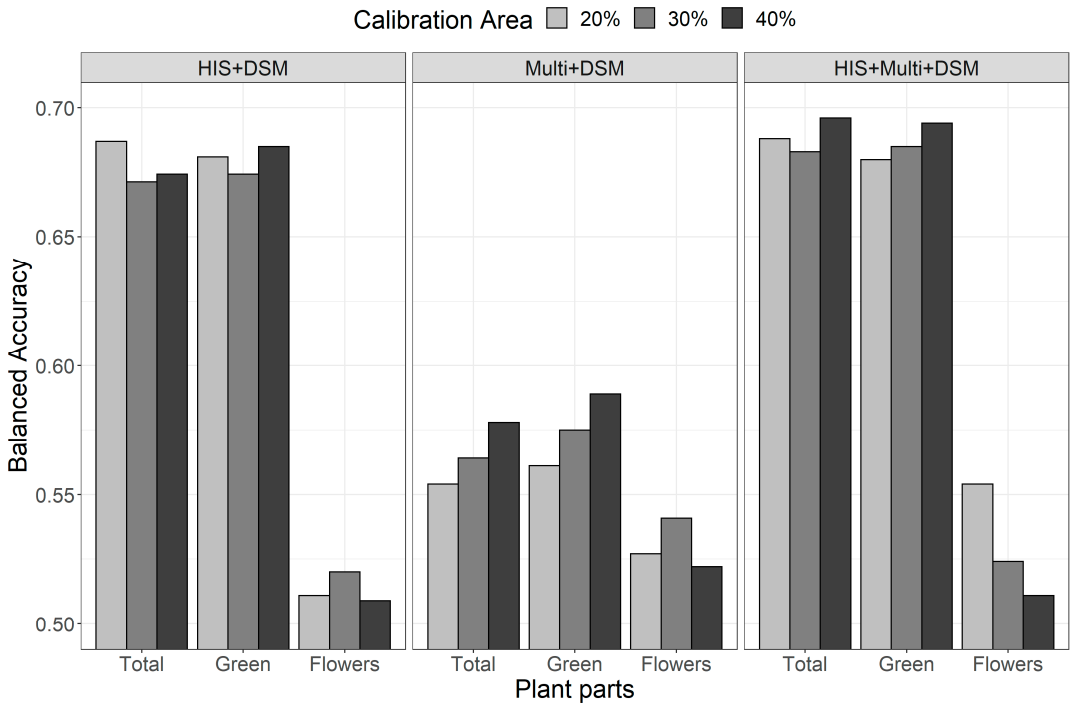

Figure 5. Outcomes of the assessment of the 27 models expressed as balanced accuracy (BA).

Table 1. Results of the linear model using balanced accuracy (BA) as the response variable and the dataset factors of variable (*Set*), plant part (*Part*) and percentage of calibration area (*Cal. Area*) as covariates. Values are reported as mean estimate and 95% confidence interval. Only the interactions between the factors that were found to significantly affect BA are shown. The reference levels are HIS + DSM for *Set*, Total for *Part* and 30% for *Cal. Area*. Significance is reported as *** $p < 0.001$.

	Mean	**95% CI**
Set Multi + DSM	−0.112 ***	−0.131, −0.093
Set HIS + Multi + DSM	0.012	−0.007, 0.031
Part Green	0.003	−0.016, 0.022
Part Flowers	−0.164 ***	−0.183, −0.145
Cal. Area 30%	−0.001	−0.012, 0.010
Cal. Area 40%	0.002	−0.009, 0.013
Set Multi + DSM:*Part* Green	0.007	−0.020, 0.034
Set HIS + Multi + DSM:*Part* Green	−0.005	−0.032, 0.022
Set Multi + DSM:*Part* Flowers	0.129 ***	0.102, 0.156
Set HIS + Multi + DSM:*Part* Flowers	0.005	−0.022, 0.032
Constant	0.677 ***	0.662, 0.692
Observations	27	
R^2	0.984	
Adjusted R^2	0.974	
Residual Std. Error	0.012 (df = 16)	
F Statistic	98.114 *** (df = 10; 16)	

Considering the original RGB image and the manual photointerpretation, it can be appreciated that all three models tend to correctly predict the presence of *Carpobrotus* in larger areas (Figure 6). The main shape of the largest *Carpobrotus* patches was identified by all three models. At the same time, it can be seen that all models tended to predict as *Carpobrotus*, a group of plants visible in the bottom right-hand corner, which are, however, other species (Figure 6). Finally, it can be seen that the HIS + DSM and especially Multi +

DSM models, identified many patches—especially very small ones—as *Carpobrotus*, a trend that was visually less pronounced in the HIS + Multi + DSM model.

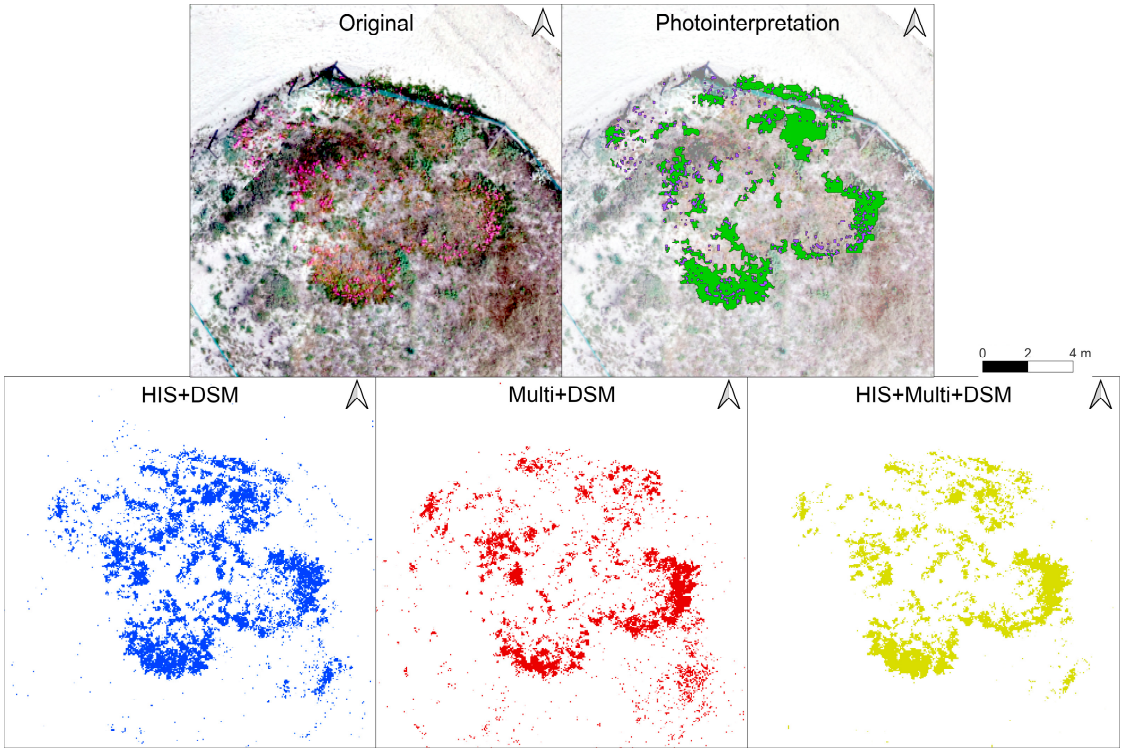

Figure 6. Example image showing results of the prediction of total *Carpobrotus* using the intermediate training area (30%) and the datasets HIS + DSM, Multi + DSM, and HIS + Multi + DSM. All images have the same scale, while the different colours are used only to aid visualization. The original orthomosaic at 5 cm resolution is shown in the top left, while the manual photointerpretation is visible in the top right. The figure shows a typical *Carpobrotus* patch surrounded by bare sand and other dune vegetation. Compared with the original RGB mosaic and manual photointerpretation, several parts of the image were misinterpreted as *Carpobrotus*, especially by the models based on HIS + DSM and Multi + DSM, while HIS + Multi + DSM retained the overall shape of the *Carpobrotus* patch.

In terms of variable importance (Figure 7), when using HIS + DSM data, intensity (INT) was the most important variable in predicting both Total and Green parts, while saturation (SAT) was predominant for Flowers. Concerning the Multi + DSM dataset, the importance of the variables was comparable between the different parts of the plant, with GNDVI marginally more important than SAVI. Finally, for the more complex dataset, HIS + Multi + DSM, intensity, saturation and GNDVI each contributed 1/5 of the importance of the overall variables in the case of Total and Green parts, while GNDVI was more relevant in the case of Flowers. Although DSM was the only variable included in all models, its importance was always marginal, exceeding 25% only in the case of Flowers in Multi + DSM.

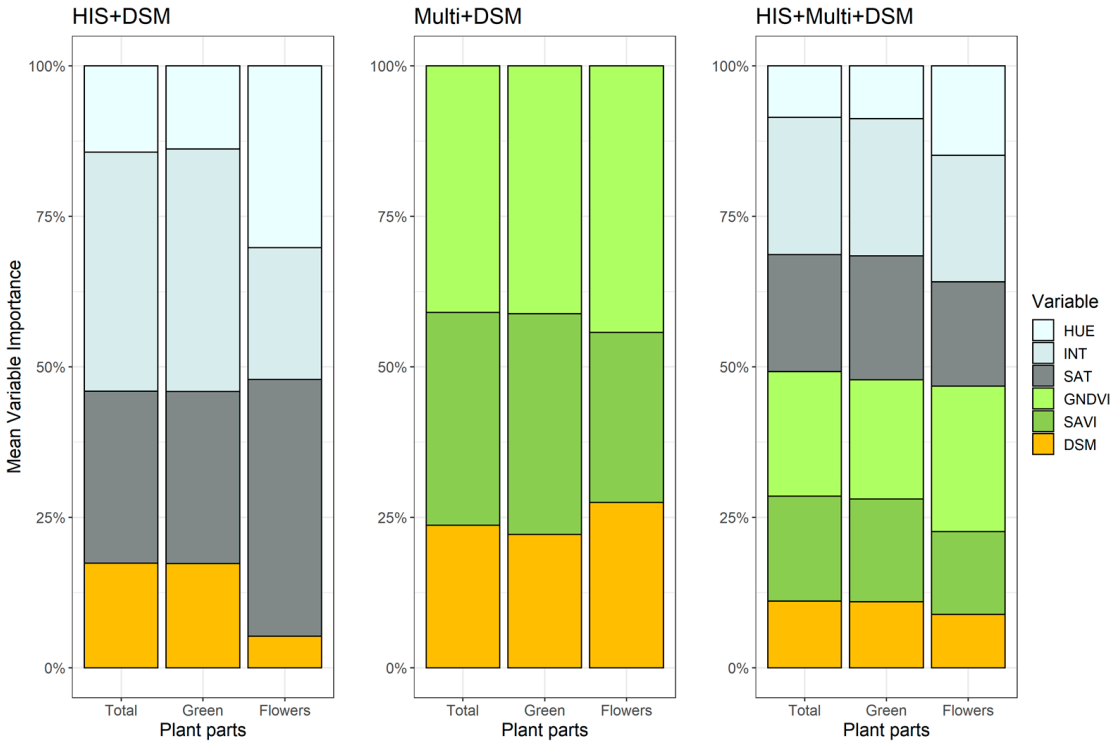

Figure 7. Importance of variables in different datasets and for different parts of the plant. Data for the intermediate calibration set (30%) are shown.

4. Discussion

4.1. On the Best Set of Variables to Predict the Presence of Carpobrotus

Balanced accuracy (BA) is one of the most robust metrics when class imbalance is present in the data [74,82]. As the average of sensitivity and specificity, BA is an unbiased metric ranging between 0 and 1 that outperforms classic metrics such as overall accuracy or Kappa with imbalanced data [82]. In our case, the class imbalance was conspicuous, as absences were more than 50 times more abundant than presences for Total and Green parts, and up to 4000 times for Flowers. Moreover, when the target species (e.g., an invasive alien plant) covers only a small portion of the studied area and there is no interest in mapping other classes, general agreement metrics (such as overall accuracy and Kappa) can be misleading [39,83].

Our results showed that the highest BA was reached by using a combination of RGB-derived variables along with data derived from multispectral sensors, with only a partial contribution from terrain morphology (DSM).

Both intensity and saturation were important variables in explaining the presence of *Carpobrotus*, while in comparison, for *Acacia saligna* (Labill.) H.L.Wendl. (Fabaceae) hue was more important in the absence of flowers, and saturation during flowering [34]. In general, even simple RGB images without the contribution of multispectral data have been shown to be viable instruments in detecting IAPs when the ultra-high-definition of UAVs is available [37,39,84,85]. Nevertheless, the integration of multispectral-derived indexes improved the prediction, as was also shown for other IAPs [34,39,85–87]. Even though NDVI was used in several cases [34,38,40,68,87], we used a modified version of NDVI based on near-infrared and green bands rather than near-infrared and red bands. This index (GNDVI) contributed to improving our predictions, and was also shown to be an effective and promising predictor when dealing with direct and indirect effects of invasive species, as it has even been used in monitoring vegetation health following invasion of pests [40,88,89]. Mallmann et al. found that spectral indexes that have a biochemical purpose, such as GNDVI, were the most effective in predicting the presence of invasive trees such as *Psidium*

guajava L. (Myrtaceae) and *Ligustrum lucidum* W.T.Aiton (Oleaceae; [32]). Similarly, GNDVI was shown to be a good predictor for monitoring the invasive *Acacia mangium* Willd. (Fabaceae) given its capability to differentiate active photosynthetic vegetation from other surface types, such as bare soils [33].

In contrast with previous research, DSM did not substantially contribute to discriminating *Carpobrotus* from the surrounding vegetation. Given its creeping habit, *Carpobrotus* does not rise substantially above the surrounding vegetation and at least based on our results, it does not appear to be particularly correlated with areas of higher or lower dune morphology. Moreover, invasion from *Carpobrotus* has been shown to homogenize horizontal vegetative cover [90]. In comparison, DSM was shown to be an important predictor for invasive trees, especially when flowers are not present, as the tree-like habitus raises the plants above the surrounding vegetation [34]. Accordingly, DSM was shown to be pivotal in discriminating between trees and shrubs [68] and even for identifying weeds from crops in precision agriculture applications [44].

Deriving BA from TSS values, in predicting the presence of the invasive alien *Acacia saligna* using UAV images, Marzialetti et al. reached values between 0.77 and 0.82 in preflowering and between 0.83 and 0.88 in flowering plants [34]. These BA values were larger than we achieved with *Carpobrotus*, but the differences in life-form and plant size must be considered.

Hamylton et al. used UAV-derived imagery at a spatial resolution of 3 cm and machine learning (convolutional neural network) to map the presence of a tussock native species (*Lomandra longifolia* Labill., Asparagaceae) introduced following invasive alien species eradication operations [91]. Their approach (which also compared pixel-based and manual digitisation techniques) produced optimal results using machine learning, highlighting the advantages of the latter approach in mapping individual plants [91]. Although our results also showed that a machine learning approach is appropriate for a species such as *Carpobrotus*, it should be borne in mind that a species such as *L. longifolia* forms very well-defined patches in terms of shape and size compared to a creeping herbaceous species such as *Carpobrotus*.

UAV was also used to monitor the invasive climbing vine *Mikania micrantha* Kunth. (Asteraceae) that forms large and compact patches on the cliffs of a small island off the southern coast of China [37]. Using only an integrative approach of 2D and 3D RGB imagery, Wu et al. demonstrated that, despite limited spectral information, ultra-high resolution UAV mosaics could effectively improve texture effectiveness in invasive mapping plants [37], a result that was not matched in our case although the morphology of our dunes was much less articulated than the steep walls of an island. The area under investigation was a sector of central Italy on the Thyrrenian coast (41.909461°N, 12.148823°E, Passoscuro, Fiumicino, Rome; Figure 2). In this area, it is possible to recognise the typical dune zonation characterised by strong environmental gradients from the coastline inland that contribute to the formation of a sequence of habitats, many of which are of conservation importance [3,13,14]. In spite of the presence of a well-formed dune structure, the Passoscuro area has also been subject to tourist exploitation, encouraging a strong colonisation of alien species, in particular *Carpobrotus* [41].

4.2. On the Prediction of the Whole Plant or Its Vegetative/Reproductive Parts

We implemented an iterative procedure to optimize the segmentation of an herbaceous IAP such as *Carpobrotus*, which led to consistent results, especially regarding the whole plant or only the green parts. The LSMS algorithm implemented in Orfeo Toolbox is designed for the segmentation of very high resolution images by returning a segmented image that contains the radiometric mean and variance of each band [68]. There is still comparatively scarce literature on LSMS applied to UAV images [34,68], especially on an extremely fine scale as the one we adopted. The three optimized parameters (spatial radius, range radius, and minimum segment size) can be considered functional to image smoothing (based on spatial detail), segmentation (based on spectral detail) and merging of segments,

respectively [68,80,86]. In more detail, the spectral radius is the spectral signature distance between the bands and is expressed in radiometric units based on the Euclidean distance between the spectral signature values of the pixels [68]. De Luca et al. found that the optimal range radius for segmenting cork oak woodlands was six, because lower values led to over-segmentation and higher values to under-segmentation [68]. Marzialetti et al., instead, used a value of five for segmenting the invasive alien species *Acacia saligna* [34]. Both cases can be compared to our study as they used LSMS segmentation based on UAV images, yet they were both based on segmenting larger objects such as trees. The segmentation of smaller objects such as *Carpobrotus* plants led to results that varied according to the dataset used and the parts analysed. In particular, *Carpobrotus* flowers are showy and comparatively large for Aizoaceae, with a mean reported diameter of 7 cm [49], but can reach up to 12 cm in their invasive areas [92]. However, single flowers could be reduced to one or two pixels even with our 5 cm spatial resolution, resulting in inconstant LSMS parameters according to the dataset used and poorer results in terms of the performance of the models.

4.3. On the Minimum Size of the Training Area

Photointerpretation was carried out over the entire area to obtain the best overview of the calibrated model using machine learning to optimise and automate the procedure and minimising manual digitisation. In fact, although expert-based photointerpretation is certainly one of the best approaches, it is undoubtedly also one of the most time-consuming and operationally demanding compared to semi-automatic machine-learning-based classification systems, thus it is necessary to identify an optimal trade-off between the two methods depending on the study system [85,87,91,93]. Consequently, identifying the minimum area where manual digitisation should be carried out appears to be of great importance. Values of training objects ranging between 22% and 30% of the total surveyed area have been reported in literature when dealing with invasive plants [39,44], although in the case of larger plants (such as trees) this value can be as low as 2% [34]. In our case, we found that the effect of incrementing the training data from 20% to 40% was not significant. Therefore, especially when the area to be monitored is very large and the effort required for photointerpretation is to be reduced, values of approximately 20% may be adequate to calibrate optimal models. However, it seems more prudent and in line with previous literature on herbaceous plants to recommend the intermediate threshold of 30%.

4.4. Remarks on Previous RS Research on Carpobrotus and Some of Their Biological/Ecological Features

Carpobrotus can have severe negative effects on invaded ecosystems [53,54] and, as it happens also with other alien species on sandy beaches, its presence may have detrimental effects on ecosystem services [3,11,16]. Thus, effective and low-cost early detection strategies by means of RS remain pivotal for containing IAPs [29,34–36], including *Carpobrotus*. Yet, research on *Carpobrotus* through remote sensing is limited. Some studies used field collected surveys on dune ecosystems invaded by *Carpobrotus* and explored them by means of remote sensing data. Marzialetti et al. used field data of dune communities (both invaded and not-invaded by *Carpobrotus*) in order to explore whether spectral diversity can provide reliable information for monitoring floristic diversity even in ecosystems altered by plant invasions [48]. Similarly, Malavasi et al. used data from field surveys to explore the effect of high-resolution optical imagery and three-dimensional topographic models obtained from LiDAR on the presence of five IAPs, including *Carpobrotus* [41].

However, studies aimed at directly surveying *Carpobrotus* by remote sensing are still very few, especially regarding the use of UAVs, and in this respect, our contribution represents a turning point. Bogdan et al. studied the population size of *Carpobrotus* invading cliffs in Israel [49]. On a smaller area (about 2 ha) but with a higher spatial resolution (35 mm), Bogdan et al. used UAV images to study the population size of *Carpobrotus*

through manual digitizing of the main patches during two years of observation, in order to develop parameters for a demographic model [49].

Underwood et al. used hyperspectral imagery derived from an airborne visible/infrared imaging spectrometer to map *Carpobrotus edulis* and another invasive grass (*Cortaderia jubata* (Lemoine) Stapf, Poaceae) along the central coast of California [47,50]. Although the approach of Underwood et al. gave very encouraging results, especially since the hyperspectral data made it possible to more accurately identify the presence of water in succulent leaves, their method was at a larger spatial scale (4.5 m) and resulted primarily in classifying habitats with different degrees of *Carpobrotus* invasion rather than individual plants [47]. Moreover, it must be taken into account that the use of aircrafts is more expensive and requires greater technical experience when compared to UAVs, which are light, inexpensive and require minimal experience to operate [29,36,49,60].

Looking at the predictive comparison of the different models applied to a typical *Carpobrotus* patch, neither HIS + DSM nor Multi + DSM was able to provide sufficient discriminatory power to distinguish consistently between *Carpobrotus* and other vegetation with a similar spectral response. This effect was remarkably less evident with HIS + Multi + DSM, despite the BA values not being much higher than HIS + DSM. On a mere visual inspection of HIS + Multi + DSM results, plants of *Carpobrotus* were identified correctly in most cases.

Carpobrotus is a difficult species to map and, especially when vegetation is dense, individual plants may be hard to identify even with expert-based manual digitizing [49]. Given its growth habit and the complexity of discriminating between taxa and hybrids, *Carpobrotus* plants tend to vary both in shape and colour, depending on age and site disturbance [53,54]. Typical plants growing under ideal conditions form an almost circular shape, progressing from the centre to the edges and reaching peak growth when the plants are about 50 years old [94]. As the plants age, the older branches in the middle die off and become greyish, sometimes leaving only a torus of active vegetation (see Figure 1). Similarly, young leaves tend to have brighter colours, while older plants become more yellowish according to a change in light use efficiency, also considering that *Carpobrotus* shows a facultative C3-CAM photosynthetic strategy [54,95,96]. Moreover, some colour differences have also been attributed to the species (i.e., *C. edulis* vs. *C. acinaciformis* [53,54]). Given *Carpobrotus* strong propensity toward clonal reproduction over seed dispersal [52,53,95], even a few plant fragments can give rise to new patches. In disturbed environments, there can thus be numerous small patches of *Carpobrotus* [54], often without flowers, making them difficult to identify. In addition, because *Carpobrotus* depletes dune vegetation and, consequently, also the presence of dune-stabilizing species such as *Thinopyrum junceum* (L.) Á.Löve and *Calamagrostis arenaria* (L.) Roth subsp. *arundinacea* (Husn.) Banfi, Galasso & Bartolucci [53,54,97], individual *Carpobrotus* plants can often appear fragmented or masked because they have been covered by sand after adverse weather events.

Considering all the above information regarding the particular challenges posed by *Carpobrotus*, the results of this study represent an excellent trade-off for a mapping protocol that is rapid, inexpensive, and can be easily repeated over time (e.g., before and after management or eradication programs). In addition, the results provided by the UAV can be seen as a solid basis to extend IAP monitoring to satellite data with metric spatial resolution, such as PlanetScope [38,98], or even satellites that can achieve sub-metric resolution such as WorldView-2 or Pleiades 1B PMS [39,40].

5. Conclusions

Given its ecology and the peculiar features of its growing environment, the case of mapping the presence of *Carpobrotus* through UAV images presented some challenges and limitations. Yet, our study represents the first comprehensive contribution to mapping *Carpobrotus* in dune ecosystems using an integrative approach of image segmentation, photointerpretation, and classification using machine learning based on UAV images. Our results allowed us to determine that a mapping protocol using UAVs must take into account

the following factors: (a) results offered by a synergistic presence of RGB and multispectral data (i.e., HIS + Multi + DSM) improve *Carpobrotus* prediction, offering better BA values and presence maps more congruent with photointerpretation, although results based only on RGB-derived data were not significantly different from those including multispectral information; (b) prediction of flowers does not appear robust when compared with the whole plant and green parts alone at a 5 cm spatial resolution, thus we recommended considering the whole plant, thus facilitating identification and mapping even during periods when the plant is not in anthesis; and (c) we found no significant differences due to the size of the training area, so even a training area corresponding to 20% of the total area appears adequate for building the models, although we recommend a more conservative threshold of 30%.

Author Contributions: Conceptualization, F.M., L.F. and M.L.C.; methodology, F.M., L.F. and W.D.S.; software, M.I., F.M., P.V.P., M.F. and M.D.F.; validation, M.I., F.M. and M.D.F.; formal analysis, M.I. and M.D.F.; investigation, F.M., L.F. and W.D.S.; resources, A.T.R.A. and M.L.C.; data curation, M.I. and M.D.F.; writing—original draft preparation, M.I.; writing—review and editing, M.I., F.M., M.D.F., A.T.R.A., W.D.S., L.F., P.V.P. and M.L.C.; visualization, M.I. and M.L.C.; supervision, M.L.C.; project administration, A.T.R.A. and M.L.C. All authors have read and agreed to the published version of the manuscript.

Funding: This research received no external funding.

Data Availability Statement: The data presented in this study are available on request from the corresponding author.

Acknowledgments: This research was supported by Project DM 1062-10/08/2021, RTD-A (Action IV.6: Green. Code: 39-G-13537-2), PON-AIM (Programma Operativo Nazionale ricerca e innovazione 2014–2020; ID AIM1897595-2), and bilateral program Italy–Israel DERESEMII (Developing state-of-the-art remote sensing tools for monitoring the impact of invasive plant). The authors are grateful to Federica Pontieri for her support. The authors acknowledge the editor and the three anonymous reviewers for the appreciation and helpful comments that help us to improve the manuscript.

Conflicts of Interest: The authors declare no conflict of interest.

References

1. Agardy, T.; Alder, J. Chapter 19: Coastal Systems. In *Ecosystems and Human Well-Being: Current State and Trends, Volume 1*; Routledge: London, UK, 2005; pp. 17–38.
2. Crain, C.M.; Halpern, B.S.; Beck, M.W.; Kappel, C.V. Understanding and Managing Human Threats to the Coastal Marine Environment. *Ann. N. Y. Acad. Sci.* **2009**, *1162*, 39–62. [CrossRef] [PubMed]
3. Carboni, M.; Carranza, M.L.; Acosta, A. Assessing conservation status on coastal dunes: A multiscale approach. *Landsc. Urban Plan.* **2009**, *91*, 17–25. [CrossRef]
4. Menicagli, V.; Balestri, E.; Biale, G.; Corti, A.; La Nasa, J.; Modugno, F.; Castelvetro, V.; Lardicci, C. Leached degradation products from beached microplastics: A potential threat to coastal dune plants. *Chemosphere* **2022**, *303*, 135287. [CrossRef] [PubMed]
5. Menicagli, V.; Balestri, E.; Vallerini, F.; Castelli, A.; Lardicci, C. Combined effect of plastic litter and increased atmospheric nitrogen deposition on vegetative propagules of dune plants: A further threat to coastal ecosystems. *Environ. Pollut.* **2020**, *266*, 115281. [CrossRef] [PubMed]
6. Battisti, C.; Fanelli, G.; Filpa, A.; Cerfolli, F. Giant Reed (*Arundo donax*) wrack as sink for plastic beach litter: First evidence and implication. *Mar. Pollut. Bull.* **2020**, *155*, 111179. [CrossRef]
7. Brown, A.C.; McLachlan, A. Sandy shore ecosystems and the threats facing them: Some predictions for the year 2025. *Environ. Conserv.* **2002**, *29*, 62–77. [CrossRef]
8. Malavasi, M.; Santoro, R.; Cutini, M.; Acosta, A.T.R.; Carranza, M.L. What has happened to coastal dunes in the last half century? A multitemporal coastal landscape analysis in Central Italy. *Landsc. Urban Plan.* **2013**, *119*, 54–63. [CrossRef]
9. van der Meulen, F.; Udo de Haes, H.A. Nature conservation and integrated coastal zone management in Europe: Present and future. *Landsc. Urban Plan.* **1996**, *34*, 401–410. [CrossRef]
10. Bascom, W. *Waves and Beaches*; Anchor Press/Doubleday Publishing: New York, NY, USA, 1980.
11. Drius, M.; Jones, L.; Marzialetti, F.; de Francesco, M.C.; Stanisci, A.; Carranza, M.L. Not just a sandy beach. The multi-service value of Mediterranean coastal dunes. *Sci. Total Environ.* **2019**, *668*, 1139–1155. [CrossRef]
12. Acosta, A.; Ercole, S.; Stanisci, A.; Pillar, V.D.P.; Blasi, C. Coastal vegetation zonation and dune morphology in some Mediterranean ecosystems. *J. Coast. Res.* **2007**, *23*, 1518–1524. [CrossRef]

13. Del Vecchio, S.; Fantinato, E.; Roscini, M.; Acosta, A.T.R.; Bacchetta, G.; Buffa, G. The germination niche of coastal dune species as related to their occurrence along a sea–inland gradient. *J. Veg. Sci.* **2020**, *31*, 1114–1123. [CrossRef]
14. Fenu, G.; Carboni, M.; Acosta, A.T.R.; Bacchetta, G. Environmental Factors Influencing Coastal Vegetation Pattern: New Insights from the Mediterranean Basin. *Folia Geobot.* **2013**, *48*, 493–508. [CrossRef]
15. Marzialetti, F.; Di Febbraro, M.; Malavasi, M.; Giulio, S.; Rosario Acosta, A.T.; Carranza, M.L. Mapping coastal dune landscape through spectral Rao's Q temporal diversity. *Remote Sens.* **2020**, *12*, 2315. [CrossRef]
16. Muñoz-Vallés, S.; Cambrollé, J. The threat of native-invasive plant species to biodiversity conservation in coastal dunes. *Ecol. Eng.* **2015**, *79*, 32–34. [CrossRef]
17. Niphadkar, M.; Nagendra, H. Remote sensing of invasive plants: Incorporating functional traits into the picture. *Int. J. Remote Sens.* **2016**, *37*, 3074–3085. [CrossRef]
18. Vilà, M.; Espinar, J.L.; Hejda, M.; Hulme, P.E.; Jarošík, V.; Maron, J.L.; Pergl, J.; Schaffner, U.; Sun, Y.; Pyšek, P. Ecological impacts of invasive alien plants: A meta-analysis of their effects on species, communities and ecosystems. *Ecol. Lett.* **2011**, *14*, 702–708. [CrossRef]
19. Genovesi, P.; Shine, C. *European Strategy on Invasive Alien Species: Convention on the Conservation of European Wildlife and Habitats (Bern Convention)*; Council of Europe: London, UK, 2004; ISBN 9287154880.
20. Sitzia, T.; Campagnaro, T.; Kowarik, I.; Trentanovi, G. Using forest management to control invasive alien species: Helping implement the new European regulation on invasive alien species. *Biol. Invasions* **2016**, *18*, 1–7. [CrossRef]
21. Simpson, A.; Jarnevich, C.; Madsen, J.; Westbrooks, R.; Fournier, C.; Mehrhoff, L.; Browne, M.; Graham, J.; Sellers, E. Invasive species information networks: Collaboration at multiple scales for prevention, early detection, and rapid response to invasive alien species. *Biodiversity* **2009**, *10*, 5–13. [CrossRef]
22. Yemshanov, D.; Haight, R.G.; Koch, F.H.; Venette, R.C.; Swystun, T.; Fournier, R.E.; Marcotte, M.; Chen, Y.; Turgeon, J.J. Optimizing surveillance strategies for early detection of invasive alien species. *Ecol. Econ.* **2019**, *162*, 87–99. [CrossRef]
23. Bradley, B.A. Remote detection of invasive plants: A review of spectral, textural and phenological approaches. *Biol. Invasions* **2014**, *16*, 1411–1425. [CrossRef]
24. Dai, J.; Roberts, D.A.; Stow, D.A.; An, L.; Hall, S.J.; Yabiku, S.T.; Kyriakidis, P.C. Mapping understory invasive plant species with field and remotely sensed data in Chitwan, Nepal. *Remote Sens. Environ.* **2020**, *250*, 112037. [CrossRef]
25. Huang, C.; Asner, G.P. Applications of remote sensing to alien invasive plant studies. *Sensors* **2009**, *9*, 4869–4889. [CrossRef] [PubMed]
26. Peerbhay, K.; Mutanga, O.; Lottering, R.; Ismail, R. Mapping *Solanum mauritianum* plant invasions using WorldView-2 imagery and unsupervised random forests. *Remote Sens. Environ.* **2016**, *182*, 39–48. [CrossRef]
27. Masemola, C.; Cho, M.A.; Ramoelo, A. Sentinel-2 time series based optimal features and time window for mapping invasive Australian native *Acacia* species in KwaZulu Natal, South Africa. *Int. J. Appl. Earth Obs. Geoinf.* **2020**, *93*, 102207. [CrossRef]
28. Ishii, J.; Washitani, I. Early detection of the invasive alien plant *Solidago altissima* in moist tall grassland using hyperspectral imagery. *Int. J. Remote Sens.* **2013**, *34*, 5926–5936. [CrossRef]
29. Vaz, A.S.; Alcaraz-Segura, D.; Campos, J.C.; Vicente, J.R.; Honrado, J.P. Managing plant invasions through the lens of remote sensing: A review of progress and the way forward. *Sci. Total Environ.* **2018**, *642*, 1328–1339. [CrossRef] [PubMed]
30. Oldeland, J.; Revermann, R.; Luther-Mosebach, J.; Buttschardt, T.; Lehmann, J.R.K. New tools for old problems—comparing drone- and field-based assessments of a problematic plant species. *Environ. Monit. Assess.* **2021**, *193*, 90. [CrossRef]
31. Rende, S.F.; Bosman, A.; Di Mento, R.; Bruno, F.; Lagudi, A.; Irving, A.D.; Dattola, L.; Giambattista, L.D.; Lanera, P.; Proietti, R.; et al. Ultra-High-Resolution Mapping of *Posidonia oceanica* (L.) Delile Meadows through Acoustic, Optical Data and Object-based Image Classification. *J. Mar. Sci. Eng.* **2020**, *8*, 647. [CrossRef]
32. Mallmann, C.L.; Zaninni, A.F.; Pereira Filho, W. Vegetation index based in unmanned aerial vehicle (UAV) to improve the management of invasive plants in Protected Areas, Southern Brazil. *Int. Arch. Photogramm. Remote Sens. Spat. Inf. Sci.-ISPRS Arch.* **2020**, *42*, 521–524. [CrossRef]
33. Lehmann, J.R.K.; Prinz, T.; Ziller, S.R.; Thiele, J.; Heringer, G.; Meira-Neto, J.A.A.; Buttschardt, T.K. Open-Source Processing and Analysis of Aerial Imagery Acquired with a Low-Cost Unmanned Aerial System to Support Invasive Plant Management. *Front. Environ. Sci.* **2017**, *5*, 1–16. [CrossRef]
34. Marzialetti, F.; Frate, L.; De Simone, W.; Frattaroli, A.R.; Acosta, A.T.R.; Carranza, M.L. Unmanned Aerial Vehicle (UAV)-Based Mapping of *Acacia saligna* Invasion in the Mediterranean Coast. *Remote Sens.* **2021**, *13*, 3361. [CrossRef]
35. de Sá, N.C.; Castro, P.; Carvalho, S.; Marchante, E.; López-Núñez, F.A.; Marchante, H. Mapping the Flowering of an Invasive Plant Using Unmanned Aerial Vehicles: Is There Potential for Biocontrol Monitoring? *Front. Plant Sci.* **2018**, *9*, 1–13. [CrossRef] [PubMed]
36. Hill, D.J.; Tarasoff, C.; Whitworth, G.E.; Baron, J.; Bradshaw, J.L.; Church, J.S. Utility of unmanned aerial vehicles for mapping invasive plant species: A case study on yellow flag iris (*Iris pseudacorus* L.). *Int. J. Remote Sens.* **2017**, *38*, 2083–2105. [CrossRef]
37. Wu, Z.; Ni, M.; Hu, Z.; Wang, J.; Li, Q.; Wu, G. Mapping invasive plant with UAV-derived 3D mesh model in mountain area—A case study in Shenzhen Coast, China. *Int. J. Appl. Earth Obs. Geoinf.* **2019**, *77*, 129–139. [CrossRef]
38. Marzialetti, F.; Di Febbraro, M.; Frate, L.; De Simone, W.; Acosta, A.T.R.; Carranza, M.L. Synergetic use of unmanned aerial vehicle and satellite images for detecting non-native tree species: An insight into *Acacia saligna* invasion in the Mediterranean coast. *Front. Environ. Sci.* **2022**, *10*, 1–15. [CrossRef]

39. Martin, F.-M.; Müllerová, J.; Borgniet, L.; Dommanget, F.; Breton, V.; Evette, A. Using Single- and Multi-Date UAV and Satellite Imagery to Accurately Monitor Invasive Knotweed Species. *Remote Sens.* **2018**, *10*, 1662. [CrossRef]
40. Alvarez-Taboada, F.; Paredes, C.; Julián-Pelaz, J. Mapping of the Invasive Species *Hakea sericea* Using Unmanned Aerial Vehicle (UAV) and WorldView-2 Imagery and an Object-Oriented Approach. *Remote Sens.* **2017**, *9*, 913. [CrossRef]
41. Malavasi, M.; Barták, V.; Jucker, T.; Acosta, A.T.R.; Carranza, M.L.; Bazzichetto, M. Strength in Numbers: Combining Multi-Source Remotely Sensed Data to Model Plant Invasions in Coastal Dune Ecosystems. *Remote Sens.* **2019**, *11*, 275. [CrossRef]
42. Giulio, S.; Cao Pinna, L.; Carboni, M.; Marzialetti, F.; Acosta, A.T.R. Invasion success on European coastal dunes. *Plant Sociol.* **2021**, *58*, 29–39. [CrossRef]
43. Giulio, S.; Acosta, A.T.R.; Carboni, M.; Campos, J.A.; Chytrý, M.; Loidi, J.; Pergl, J.; Pyšek, P.; Isermann, M.; Janssen, J.A.M.; et al. Alien flora across European coastal dunes. *Appl. Veg. Sci.* **2020**, *23*, 317–327. [CrossRef]
44. de Castro, A.; Torres-Sánchez, J.; Peña, J.; Jiménez-Brenes, F.; Csillik, O.; López-Granados, F. An Automatic Random Forest-OBIA Algorithm for Early Weed Mapping between and within Crop Rows Using UAV Imagery. *Remote Sens.* **2018**, *10*, 285. [CrossRef]
45. Wang, S.; Han, Y.; Chen, J.; Pan, Y.; Cao, Y.; Meng, H. A transfer-learning-based feature classification algorithm for UAV imagery in crop risk management. *Desalin. Water Treat* **2020**, *181*, 330–337. [CrossRef]
46. Lass, L.W.; Prather, T.S.; Glenn, N.F.; Weber, K.T.; Mundt, J.T.; Pettingill, J. A review of remote sensing of invasive weeds and example of the early detection of spotted knapweed (*Centaurea maculosa*) and babysbreath (*Gypsophila paniculata*) with a hyperspectral sensor. *Weed Sci.* **2005**, *53*, 242–251. [CrossRef]
47. Underwood, E.; Ustin, S.; DiPietro, D. Mapping nonnative plants using hyperspectral imagery. *Remote Sens. Environ.* **2003**, *86*, 150–161. [CrossRef]
48. Marzialetti, F.; Cascone, S.; Frate, L.; Di Febbraro, M.; Acosta, A.T.R.; Carranza, M.L. Measuring Alpha and Beta Diversity by Field and Remote-Sensing Data: A Challenge for Coastal Dunes Biodiversity Monitoring. *Remote Sens.* **2021**, *13*, 1928. [CrossRef]
49. Bogdan, A.; Levin, S.C.; Salguero-Gómez, R.; Knight, T.M. Demographic analysis of an Israeli *Carpobrotus* population. *PLoS ONE* **2021**, *16*, e0250879. [CrossRef]
50. Underwood, E.C.; Ustin, S.L.; Ramirez, C.M. A comparison of spatial and spectral image resolution for mapping invasive plants in coastal California. *Environ. Manag.* **2007**, *39*, 63–83. [CrossRef]
51. Roiloa, S.R.; Rodríguez-Echeverría, S.; de la Peña, E.; Freitas, H. Physiological integration increases the survival and growth of the clonal invader *Carpobrotus edulis*. *Biol. Invasions* **2010**, *12*, 1815–1823. [CrossRef]
52. Roiloa, S.R.; Abalde, S.; Xu, C.-Y.; López, L. The effect of stolon fragmentation on the colonization of clonal invasive *Carpobrotus edulis* in a coastal dune system: A field test. *Plant Species Biol.* **2017**, *32*, 460–465. [CrossRef]
53. Campoy, J.G.; Acosta, A.T.R.; Affre, L.; Barreiro, R.; Brundu, G.; Buisson, E.; González, L.; Lema, M.; Novoa, A.; Retuerto, R.; et al. Monographs of invasive plants in Europe: *Carpobrotus*. *Bot. Lett.* **2018**, *165*, 440–475. [CrossRef]
54. Sarmati, S.; Conti, L.; Acosta, A.T.R. *Carpobrotus acinaciformis* vs *Carpobrotus edulis*: Are there any differences in their impact on coastal dune plant biodiversity? *Flora* **2019**, *257*, 151422. [CrossRef]
55. Chenot, J.; Affre, L.; Passetti, A.; Buisson, E. Consequences of iceplant (*Carpobrotus*) invasion on the vegetation and seed bank structure on a Mediterranean island: Response elements for their local eradication. *Acta Bot. Gall.* **2014**, *161*, 301–308. [CrossRef]
56. Blasi, C.; Carli, E.; Celesti-Grapow, L.; Copiz, R.; Frondoni, R.; Iberite, M.; Tilia, A. *Linee Guida per la Gestione Delle Specie Vegetali Alloctone*; Manuali e Linee Guida n. 200/2022: Ispra, Italy, 2022; ISBN 978-88-448-1135-8.
57. Celesti-Grapow, L.; Abbate, G.; Baccetti, N.; Capizzi, D.; Carli, E.; Copiz, R.; Frondoni, R.; Giunti, M.; Gotti, C.; Iberite, M.; et al. Control of invasive species for the conservation of biodiversity in Mediterranean islands. The LIFE PonDerat project in the Pontine Archipelago, Italy. *Plant Biosyst.-Int. J. Deal. All Asp. Plant Biol.* **2017**, *151*, 795–799. [CrossRef]
58. Ruffino, L.; Krebs, E.; Passetti, A.; Aboucaya, A.; Affre, L.; Fourcy, D.; Lorvelec, O.; Barcelo, A.; Berville, L.; Bigeard, N.; et al. Eradications as scientific experiments: Progress in simultaneous eradications of two major invasive taxa from a Mediterranean island. *Pest Manag. Sci.* **2015**, *71*, 189–198. [CrossRef]
59. Turner, D.; Lucieer, A.; Watson, C. An Automated Technique for Generating Georectified Mosaics from Ultra-High Resolution Unmanned Aerial Vehicle (UAV) Imagery, Based on Structure from Motion (SfM) Point Clouds. *Remote Sens.* **2012**, *4*, 1392–1410. [CrossRef]
60. Mancini, F.; Dubbini, M.; Gattelli, M.; Stecchi, F.; Fabbri, S.; Gabbianelli, G. Using Unmanned Aerial Vehicles (UAV) for High-Resolution Reconstruction of Topography: The Structure from Motion Approach on Coastal Environments. *Remote Sens.* **2013**, *5*, 6880–6898. [CrossRef]
61. Moreno, J.F.; Melia, J. An optimum interpolation method applied to the resampling of NOAA AVHRR data. *IEEE Trans. Geosci. Remote Sens.* **1994**, *32*, 131–151. [CrossRef]
62. Xie, Y.; Sha, Z.; Yu, M. Remote sensing imagery in vegetation mapping: A review. *J. Plant Ecol.* **2008**, *1*, 9–23. [CrossRef]
63. Gitelson, A.A.; Kaufman, Y.J.; Merzlyak, M.N. Use of a green channel in remote sensing of global vegetation from EOS-MODIS. *Remote Sens. Environ.* **1996**, *58*, 289–298. [CrossRef]
64. Taddeo, S.; Dronova, I.; Harris, K. Greenness, texture, and spatial relationships predict floristic diversity across wetlands of the conterminous United States. *ISPRS J. Photogramm. Remote Sens.* **2021**, *175*, 236–246. [CrossRef]
65. Heute, A.R. A Soil-Adjusted Vegetation Index (SAVI). *Remote Sens. Environ.* **1988**, *25*, 295–309. [CrossRef]
66. Halmy, M.W.A.; Fawzy, M.; Ahmed, D.A.; Saeed, N.M.; Awad, M.A. Monitoring and predicting the potential distribution of alien plant species in arid ecosystem using remotely-sensed data. *Remote Sens. Appl. Soc. Environ.* **2019**, *13*, 69–84. [CrossRef]

67. Immitzer, M.; Vuolo, F.; Atzberger, C. First Experience with Sentinel-2 Data for Crop and Tree Species Classifications in Central Europe. *Remote Sens.* **2016**, *8*, 166. [CrossRef]
68. De Luca, G.; Silva, J.M.N.; Cerasoli, S.; Araújo, J.; Campos, J.; Di Fazio, S.; Modica, G. Object-Based Land Cover Classification of Cork Oak Woodlands using UAV Imagery and Orfeo ToolBox. *Remote Sens.* **2019**, *11*, 1238. [CrossRef]
69. Michel, J.; Youssefi, D.; Grizonnet, M. Stable Mean-Shift Algorithm and Its Application to the Segmentation of Arbitrarily Large Remote Sensing Images. *IEEE Trans. Geosci. Remote Sens.* **2015**, *53*, 952–964. [CrossRef]
70. Suneetha, M.; Boggavarapu, L.N.; Vaddi, R.; Raja, A.R.; Gopalakrishnan, R.; Jha, C.S. Object Based Classification of Multispectral Remote Sensing Images for Forestry Applications. In Proceedings of the 2020 3rd International Conference on Image and Graphics Processing, Singapore, 8–10 February 2020; ACM: New York, NY, USA, 2020; pp. 153–157.
71. Stephens, D.; Diesing, M. A comparison of supervised classification methods for the prediction of substrate type using multibeam acoustic and legacy grain-size data. *PLoS ONE* **2014**, *9*, e93950. [CrossRef] [PubMed]
72. Kuhn, M. *Caret: Classification and Regression Training*, R package version 6.0-93; Available online: https://CRAN.R-project.org/package=caret (accessed on 1 January 2023).
73. Probst, P.; Wright, M.N.; Boulesteix, A.L. Hyperparameters and tuning strategies for random forest. *Wiley Interdiscip. Rev. Data Min. Knowl. Discov.* **2019**, *9*, e1301. [CrossRef]
74. Velez, D.R.; White, B.C.; Motsinger, A.A.; Bush, W.S.; Ritchie, M.D.; Williams, S.M.; Moore, J.H. A balanced accuracy function for epistasis modeling in imbalanced datasets using multifactor dimensionality reduction. *Genet. Epidemiol.* **2007**, *31*, 306–315. [CrossRef]
75. Congalton, R.G. A review of assessing the accuracy of classifications of remotely sensed data. *Remote Sens. Environ.* **1991**, *37*, 35–46. [CrossRef]
76. Gibson, R.; Danaher, T.; Hehir, W.; Collins, L. A remote sensing approach to mapping fire severity in south-eastern Australia using sentinel 2 and random forest. *Remote Sens. Environ.* **2020**, *240*, 111702. [CrossRef]
77. Wunderlich, R.F.; Lin, Y.-P.; Anthony, J.; Petway, J.R. Two alternative evaluation metrics to replace the true skill statistic in the assessment of species distribution models. *Nat. Conserv.* **2019**, *35*, 97–116. [CrossRef]
78. Allouche, O.; Tsoar, A.; Kadmon, R. Assessing the accuracy of species distribution models: Prevalence, kappa and the true skill statistic (TSS). *J. Appl. Ecol.* **2006**, *43*, 1223–1232. [CrossRef]
79. R Core Team. *R: A Language and Environment for Statistical Computing*; R Foundation for Statistical Computing: Vienna, Austria. Available online: https://www.r-project.org/ (accessed on 1 January 2023).
80. Gonçalves, J.; Pôças, I.; Marcos, B.; Mücher, C.A.; Honrado, J.P. SegOptim—A new R package for optimizing object-based image analyses of high-spatial resolution remotely-sensed data. *Int. J. Appl. Earth Obs. Geoinf.* **2019**, *76*, 218–230. [CrossRef]
81. Hijmans, R.J. _terra: Spatial Data Analysis_. R package version 1.6-17. Available online: https://CRAN.R-project.org/package=terra (accessed on 1 January 2023).
82. Mohammed Abdelkader, E.; Moselhi, O.; Marzouk, M.; Zayed, T. Hybrid Elman Neural Network and an Invasive Weed Optimization Method for Bridge Defect Recognition. *Transp. Res. Rec. J. Transp. Res. Board* **2021**, *2675*, 167–199. [CrossRef]
83. Pontius, R.G.; Millones, M. Death to Kappa: Birth of quantity disagreement and allocation disagreement for accuracy assessment. *Int. J. Remote Sens.* **2011**, *32*, 4407–4429. [CrossRef]
84. Kattenborn, T.; Lopatin, J.; Förster, M.; Braun, A.C.; Fassnacht, F.E. UAV data as alternative to field sampling to map woody invasive species based on combined Sentinel-1 and Sentinel-2 data. *Remote Sens. Environ.* **2019**, *227*, 61–73. [CrossRef]
85. Franklin, S.E.; Ahmed, O.S. Deciduous tree species classification using object-based analysis and machine learning with unmanned aerial vehicle multispectral data. *Int. J. Remote Sens.* **2018**, *39*, 5236–5245. [CrossRef]
86. Lourenço, P.; Teodoro, A.C.; Gonçalves, J.A.; Honrado, J.P.; Cunha, M.; Sillero, N. Assessing the performance of different OBIA software approaches for mapping invasive alien plants along roads with remote sensing data. *Int. J. Appl. Earth Obs. Geoinf.* **2021**, *95*, 102263. [CrossRef]
87. Al-Ali, Z.M.; Abdullah, M.M.; Asadalla, N.B.; Gholoum, M. A comparative study of remote sensing classification methods for monitoring and assessing desert vegetation using a UAV-based multispectral sensor. *Environ. Monit. Assess.* **2020**, *192*, 389. [CrossRef]
88. Olsson, P.-O.; Jönsson, A.M.; Eklundh, L. A new invasive insect in Sweden–*Physokermes inopinatus*: Tracing forest damage with satellite based remote sensing. *For. Ecol. Manag.* **2012**, *285*, 29–37. [CrossRef]
89. Rodrigues, J.C.V.; Cosh, M.H.; Hunt, E.R.; de Moraes, G.J.; Barroso, G.; White, W.A.; Ochoa, R. Tracking Red Palm Mite Damage in the Western Hemisphere Invasion with Landsat Remote Sensing Data. *Insects* **2020**, *11*, 627. [CrossRef] [PubMed]
90. Molinari, N.; D'Antonio, C.; Thomson, G.; Cuddington, K.; Byers, J.; Hastings, A.; Wilson, W. Carpobrotus as a case study of the complexities of species impacts. In *Ecosystem Engineers: Plants to Protists*; Academic Press: Cambridge, MA, USA, 2007; pp. 139–162.
91. Hamylton, S.M.; Morris, R.H.; Carvalho, R.C.; Roder, N.; Barlow, P.; Mills, K.; Wang, L. Evaluating techniques for mapping island vegetation from unmanned aerial vehicle (UAV) images: Pixel classification, visual interpretation and machine learning approaches. *Int. J. Appl. Earth Obs. Geoinf.* **2020**, *89*, 102085. [CrossRef]
92. Verlaque, R.; Affre, L.; Diadema, K.; Suehs, C.M.; Médail, F. Unexpected morphological and karyological changes in invasive *Carpobrotus* (Aizoaceae) in Provence (S-E France) compared to native South African species. *Comptes Rendus Biol.* **2011**, *334*, 311–319. [CrossRef]

93. Lu, D.; Weng, Q. A survey of image classification methods and techniques for improving classification performance. *Int. J. Remote Sens.* **2007**, *28*, 823–870. [CrossRef]
94. Sintes, T.; Moragues, E.; Traveset, A.; Rita, J. Clonal growth dynamics of the invasive *Carpobrotus* affine *acinaciformis* in Mediterranean coastal systems: A non-linear model. *Ecol. Modell.* **2007**, *206*, 110–118. [CrossRef]
95. Roiloa, S.R.; Rodriguez-Echeverria, S.; Lopez-Otero, A.; Retuerto, R.; Freitas, H. Adaptive plasticity to heterogeneous environments increases capacity for division of labor in the clonal invader *Carpobrotus edulis* (Aizoaceae). *Am. J. Bot.* **2014**, *101*, 1301–1308. [CrossRef]
96. Roiloa, S.R.; Rodríguez-Echeverría, S.; Freitas, H.; Retuerto, R. Developmentally-programmed division of labour in the clonal invader *Carpobrotus edulis*. *Biol. Invasions* **2013**, *15*, 1895–1905. [CrossRef]
97. Cascone, S.; Sperandii, M.G.; Cao Pinna, L.; Marzialetti, F.; Carranza, M.L.; Acosta, A.T.R. Exploring Temporal Trends of Plant Invasion in Mediterranean Coastal Dunes. *Sustainability* **2021**, *13*, 13946. [CrossRef]
98. Theron, K.J.; Pryke, J.S.; Latte, N.; Samways, M.J. Mapping an alien invasive shrub within conservation corridors using super-resolution satellite imagery. *J. Environ. Manag.* **2022**, *321*, 116023. [CrossRef]